JOURNAL OF MATERIALS SCIENCE 30 (1995) 3720–3729

The optical properties and a.c. conductivity of magnesium phosphate glasses

S. K. J. AL-ANI, I. H. O. AL-HASSANY, Z. T. AL-DAHAN
Department of Physics, College of Education for Women, University of Baghdad, Jadirya, Baghdad, Iraq

Magnesium phosphate [X MgO $-(100-X)$ P_2O_5] glasses in the composition range [$X=20$, 25, 30, 40, 45, 50 mol %] have been made. The optical properties and a.c. conductivities were measured and their amorphous nature confirmed by X-ray diffraction technique. The variation of relative density with x was anomalous. In the ultraviolet/visible regions it was found that the fundamental absorption edge is a function of glass compositions and lower absorption coefficients, $\alpha(\omega)$ follow the so-called Urbach edge. At lower absorption levels ($1 < \alpha < 10^4\ cm^{-1}$), the width of the tail of localized states in the band gap, E_g, did not vary significantly with glass composition and lay in the range (0.26–0.343) eV. In the high absorption region ($\alpha(\omega) > 10^4\ cm^{-1}$), the behaviour of $\alpha(\omega)$ suggests that there are two different transition energies for electrons in k-space, namely direct allowed transitions and non-direct transitions. In the infrared region at wavelengths $\lambda = 2.5$–30 μm, the transmission spectrum has four absorption bands. Using the Kramers–Kronig theory, the optical constants (refractive index n and extinction coefficient k) have been determined from the transmission spectrum. The a.c. conductivity, $\sigma(\omega)$, real and imaginary dielectric constants, ε_1, ε_2, and loss factor, tan δ, have been determined at room temperature in the frequency region, $\omega = 2 \times 10^4$–10^6 Hz. It has previously been established theoretically that $\sigma(\omega) \sim \omega^s$ and s was found to be in the range 0.64–0.73, depending on glass composition.

1. Introduction

For amorphous materials the optical absorption coefficient $\alpha(\omega)$, at an angular frequency of radiation ω, is related to the imaginary part of the dielectric constant $\varepsilon_2(\omega)$ by the following relation

$$\varepsilon_2(\omega) = nc\,\alpha(\omega)/\omega \quad (1)$$

where n is the refractive index and c is the speed of light in vacuum. Alternating current conductivity is of interest in that it has been observed in every amorphous semiconductor as well as in those insulators measured; in the frequency range 10–10^6 Hz the qualitative behaviour is the same, i.e.

$$\sigma(\omega) \sim \omega^s \quad (2)$$

where the exponent s is near unity ($\leqslant 1$) and is weakly temperature dependent. Such a.c. conduction behaviour is unique to the amorphous phase and is a general property for all amorphous semiconductors and insulators. The a.c. conductivity, $\sigma(\omega)$, is related to $\alpha(\omega)$, because both involve energy loss within the solid according to [1]

$$\sigma(\omega) = n\alpha(\omega)/377 \quad (3)$$

The aim of this work was to prepare magnesium phosphate (MgO–P_2O_5) glass and to measure the fundamental absorption edges in the ultraviolet/visible regions. The Kramers–Kronig relation has been applied to calculate the optical constants (n, k) from the transmission spectrum, where k is the extinction coefficient in the infrared region. The main absorption bands in this region have also been studied. The a.c. conductivity versus frequency in the range 10–10^6 Hz has also been measured and analysed.

2. Experimental procedure

2.1. Glass preparation

Analar MgO and P_2O_5 were used to prepare the glass samples. These reagents were mixed and heated in an electric furnace for about 1 h at a temperature of 400 °C; this allowed the phosphorous pentoxide to decompose and react with other batch constituents before melting would ordinarily occur. Then, the crucible with the mixture was transferred to an electric furnace at 1200 °C. After the mixture had melted, it was kept for about 2 h and stirred occasionally by an alumina rod every 20 min to ensure homogeneity and proper mixing. Each melt was cast into two mild-steel split moulds heated to a temperature 200 °C, to form glass rods 1 cm long by 1.6 cm diameter. After casting, each glass was immediately transferred to an annealing furnace, and held at a temperature of 400 °C for 1 h. The glasses were then allowed to cool to room temperature by switching the furnace off, giving an initial cooling rate of 3 °C min^{-1}.

0022–2461

2.2. Structural, density, optical and electrical measurements

X-ray diffraction measurements were made using a Philips X-ray diffractometer ($CuK_{\alpha_{1,2}}$ source, $\lambda = 0.154\,18$ nm A) and showed no peak in the diffraction pattern, which is characteristic of amorphous materials.

The density of each glass was measured as follows: A glass disc was weighed in air, ω_1, and immersed in ethyl methyl keton and reweighed, ω_2. The relative density is given by the relation [2]

$$\rho_r = 0.85\,\omega_1/(\omega_1 - \omega_2) \quad (4)$$

The optical absorption data were measured in the wavelength range $\lambda = 190$–850 nm, using a Pye–Unicam UV-Visible Spectrophotometer Model PU 8800. The absorption coefficient, $\alpha(\omega)$ was calculated from the absorbance, A, making the correction for reflection losses and using the following formula

$$\alpha(\lambda) = 2.303\,Ax^{-1} \quad (5)$$

where x is the sample thickness.

For infrared measurements the glass samples were ground in a clean mortar into a fine powder and then a small amount of glass powder was weighed and mixed with an already weighed amount of KBr powder in accordance with standard procedures [3]. The mixed powder was shaken by machine in order to obtain well-mixed powder. The pellets were formed by pressing the mixture at 10 ton for a few minutes. The pellets were of 0.65 cm radius and 0.5 mm thickness.

The infrared spectra of MgO–P_2O_5 glasses were then recorded with a pye–Unicam SP3–300 double–beam infrared spectrophotometer.

Aluminium electrodes are vacuum evaporated on two parallel faces of glass samples for electrical measurements. The samples were further annealed at 300 °C for 1 h in order to stabilize the aluminium contacts. The a.c. conductivity and dielectric constants of the samples were measured using a 4274 A LRC meter in the frequency range 2×10^4–10^6 Hz.

All the above measurements are made at room temperature. A dry atmosphere in a closed system was used to prevent any oxidation on the surface.

3. Results and discussion

3.1. Density

Fig. 1 shows the change of relative density of (MgO–P_2O_5) glasses as a function of MgO content. The results of Al-Ani and Higazy [4] are also included. From this figure the variation is anomalous. On the other hand, the present work is in agreement with previous work [4]. The (MgO–P_2O_5) (M–P) glasses have been classified by Kordes *et al.* [5] as "anomalous phosphate glasses", which exhibit anomalies in the relationship between the physical properties and M/P molar ratio around the metaphosphate composition (M/P = 1). Okura *et al.* [6] presented models to explain the phosphate glass anomaly in density, and they concluded that:

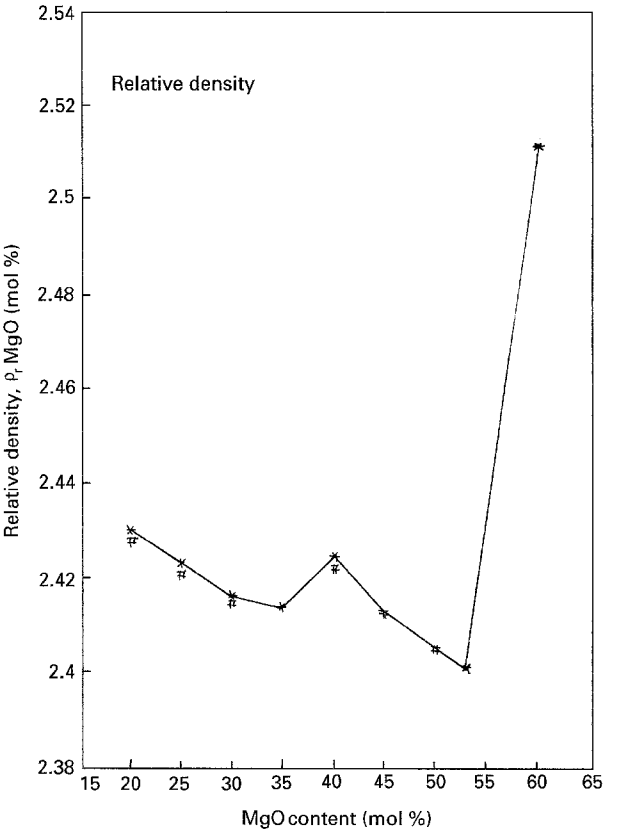

Figure 1 The relation between relative density of MgO–P_2O_5 glasses and MgO content for all X values. (#) Present results, (*) previous results [4].

1. the structure of M/P glasses is of two kinds, one includes four-membered rings of PO_4 tetrahedra at M/P < 1 (type T) while the other contains dimers of PO_4 tetrahedra at M/P > 1 (type P);
2. the calculated change in density with composition agrees with the observed result;
3. the anomaly in M/P glasses is attributed to the structural change from type T to type P around M/P = 1;
4. the phosphate glasses containing bivalent cations are divided into normal and anomalous types according to geometrical factors, namely, the size of the cation and that of the interstice formed by four PO_4 tetrahedra.

The above theoretical model [6], which accounts for the anomaly in density with MgO content around M/P = 1, is in agreement with our results for M/P = 0.6–1 (Fig. 1) but the enormous discontinuity at 53% MgO is the same as observed by Okura *et al.* around M/P = 1. The peak at 40:60 ratio is presumably within experimental error.

3.2. The fundamental absorption edge

The absorption edge of non-metallic materials gives a measure of the band strengths or energy band gap, and for crystalline materials the relationship between energy gap, E_g, and the position of the normally sharp absorption edge is

$$E_g = hc/\lambda_c \quad (6)$$

where h is Planck's constant.

The exponential dependence of the absorption coefficient $\alpha(\omega)$, on photon energy $\hbar\omega$ is found to hold over several decades for an amorphous material and takes the form

$$\alpha(\omega) = \alpha_0 \exp(\hbar\omega/E_g) \quad (7)$$

where α_0 is a constant, $\hbar$ is the reduced Planck's constant and E_g an energy which is interpreted as the width of the tail of localized states in the normally forbidden band gap, which are associated with the amorphous nature. Equation 7 was first proposed by Urbach [7] to describe the absorption edge in alkali halide crystals at high absorption level when $\alpha(\omega) \geqslant 10^4\ \mathrm{cm}^{-1}$. This relation has been found for many amorphous or glassy materials at the lower range of the absorption edge, while for higher photon energy (higher $\alpha(\omega)$) the absorption data follow a power law [1]

$$\alpha(\omega) = \frac{B}{\hbar\omega}(\hbar\omega - E_{opt})^r \quad (8)$$

and yield values of the optical energy gap, E_{opt}. B is a constant and r an index which can assume values of

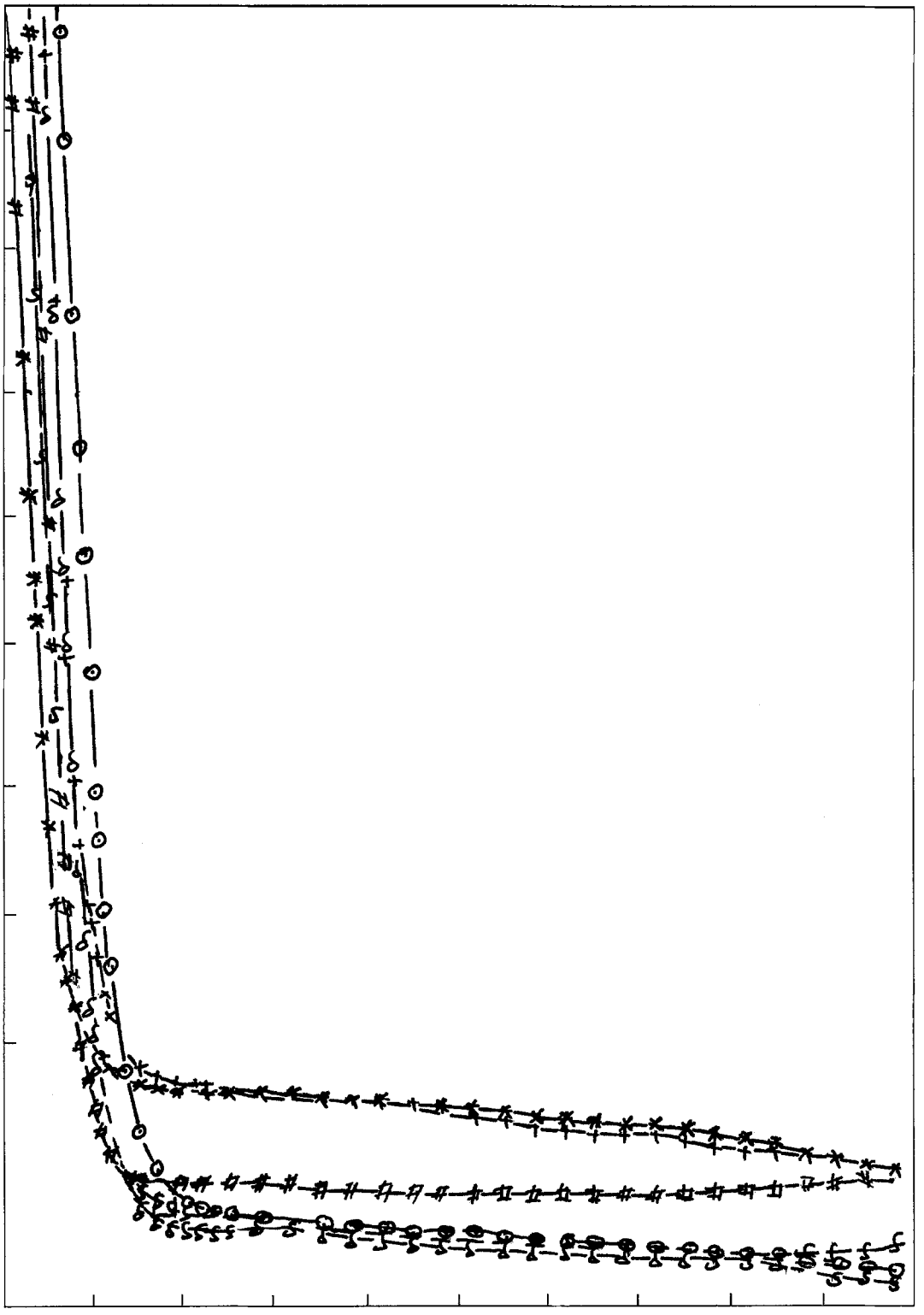

Figure 2 Optical absorbance spectrum for all X values of $MgO-P_2O_5$ glasses as a function of wavelength, λ.

1, 2, 3, 1/2 or 3/2 depending on the nature of the inter-band electronic transitions.

Equation 8 with $r = 2$ was first proposed by Tauc *et al.* [8] to represent the data of amorphous germanium films and later Davis and Mott [9] gave this general form.

Equation 8 with $r = 1$ was found to fit the optical data in amorphous selenium and $In_{30}Se_{70}$ films [10–12], whereas $r = 2$ agrees well for most thin amorphous oxide films [13–15] and for chalcogenide and oxide glasses [1, 16, 17]. Other values of the index have been found appropriate for particular amorphous materials [18–20].

Fig. 2 shows the optical absorption spectra at different compositions of $MgO–P_2O_5$ glass corrected for thickness and sample reflectivity.

It is clear that there is no sharp absorption edge and this is characteristic of the glassy state just as the X-ray diffraction spectra also show a broad featureless curve (Fig. 3).

The exponential dependence of $\alpha(\omega)$ on $\hbar\omega$ for amorphous $MgO–P_2O_5$ glass of different composition is shown in Fig. 4. The values of E_g are estimated and listed in Table I. The optical data are analysed for the higher values of $\alpha(\omega)$ above the exponential region by plotting $(\alpha\hbar\omega)^{\frac{1}{2}}$ as a function of $\hbar\omega$ for indirect transitions as shown in Fig. 5; and by plotting $(\alpha\hbar\omega)^2$ as a function of $\hbar\omega$ for direct transitions as shown in Fig. 6. The respective values of E_{opt} obtained by extrapolation to $(\alpha\hbar\omega)^{\frac{1}{2}} = 0$ and $(\alpha\hbar\omega)^2 = 0$ are also noted in Table I.

The origin of the exponential dependence of $\alpha(\omega)$ on $\hbar\omega$ in both crystalline and amorphous semiconductors is not clearly known. Dow and Redfield [21] suggested it may arise from the random fluctuations of the internal field associated with structural disorder in many amorphous solids. Tauc [22] believed that it arises from electronic transitions between localized states in the band edge tails, the density of which is assumed to fall off exponentially with energy. Davis and Mott [9] argue to the contrary. One possible reason suggested by them is that the slopes of the measured exponential edges obtained from Equation 7 are very much the same in many semiconductors, and the values of E_g for the amorphous semiconductors [1] are reported to lie between 0.045 and 0.67 eV.

As we can deduce from Figs 5 and 6 and for each glass composition, there are two optical transitions in k-space. Assuming that the lowest minimum of the conduction band and the highest maximum of the valence band lie in different regions of k-space, the direct allowed transitions may occur as in Fig. 7 and

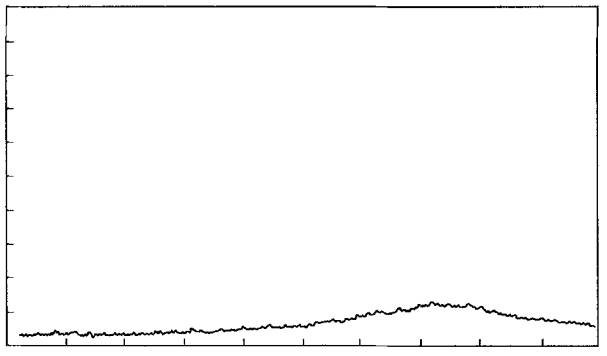

Figure 3 X-ray diffraction pattern for $MgO–P_2O_5$ glasses.

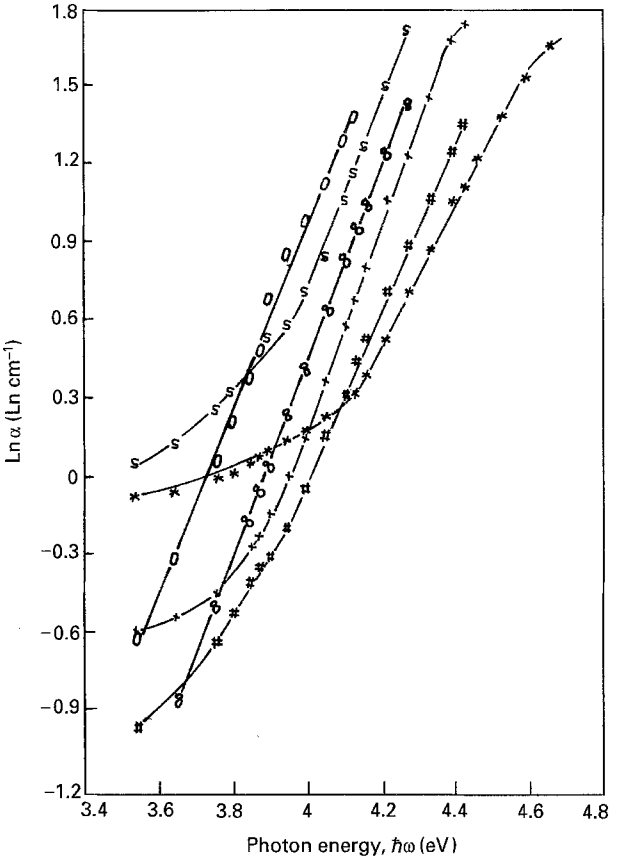

Figure 4 The relation between lnα and $\hbar\omega$ for $MgO–P_2O_5$ glasses. MgO: (*) 20%, (s) 25%, (+) 30%, (#) 40%, (&) 45%, (O) 50%.

TABLE I Some optical measurements for $MgO–P_2O_5$ glasses

X (mol%) MgO	E_{opt} (eV)		B (cm^{-1} eV^{-1}) for indirect transition	E_g (eV)	B (cm^{-1} $eV^{\frac{1}{2}}$) for direct transition
	Indirect transitions	Direct transitions			
20	3.70	4.32	29.64	0.343	40.09
25	3.64	4.09	46.69	0.293	55.42
30	3.73	4.21	49.48	0.261	53.83
40	3.65	4.24	29.64	0.300	38.58
45	3.61	4.07	32.74	0.273	39.48
50	3.44	3.94	37.34	0.268	36.93

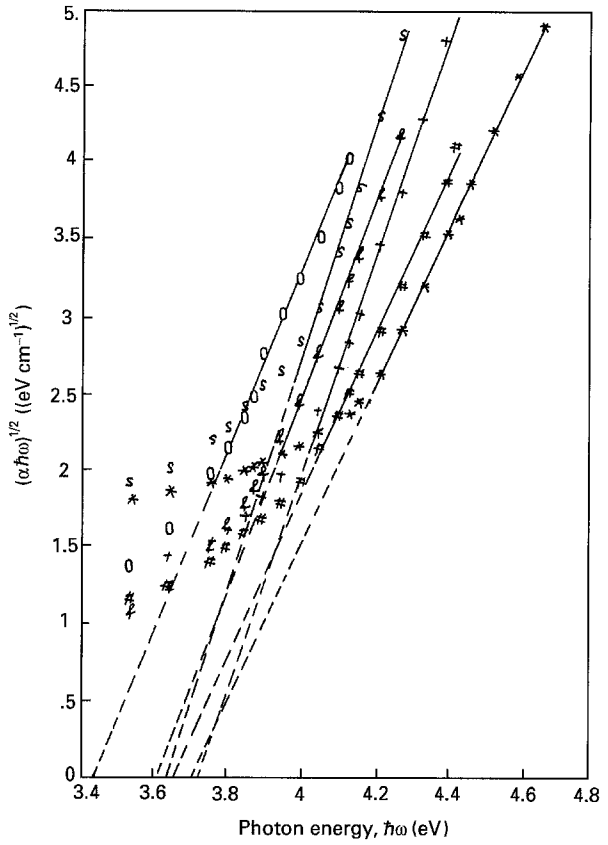

Figure 5 The relation between $(\alpha\hbar\omega)^{\frac{1}{2}}$ and $\hbar\omega$ for $MgO-P_2O_5$ glasses. MgO: (*) 20%, (s) 25%, (+) 30%, (#) 40%, (&) 45%, (○) 50%.

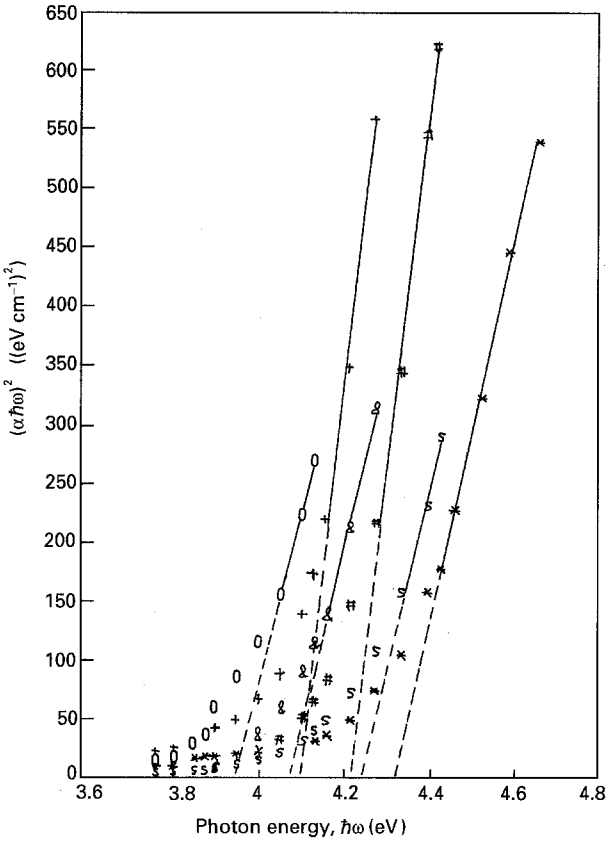

Figure 6 Relation between $(\alpha\hbar\omega)^2$ and $\hbar\omega$ for $MgO-P_2O_5$ glasses. MgO: (*) 20%, (+) 25%, (#) 30%, (s) 40%, (&) 45%, (○) 50%.

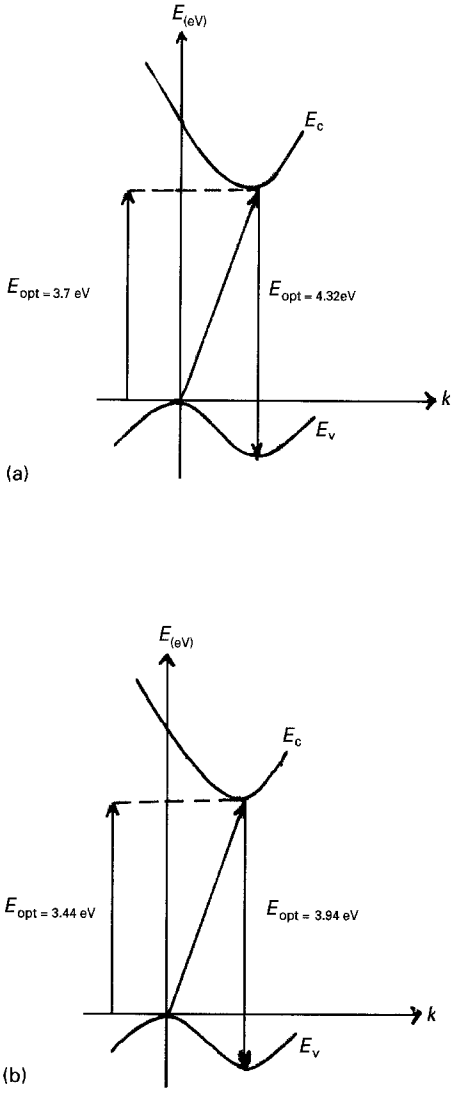

Figure 7 Suggested energy band diagrams (electron energy, E, versus wave vector, k) for $20MgO-80P_2O_5$ and $50MgO-50P_2O_5$ glasses.

the observed non-direct transitions may be associated with transitions from top of the valence band to the bottom of the conduction band.

Al-Ani and Higazy [4] confirmed these transitions in k-space and have suggested an energy band diagram for magnesium–phosphate glass as in Fig. 7.

3.3. Infrared transmission bands

Fig. 8 shows infrared transmission spectra of magnesium phosphate glasses in the wave number range 500–2000 cm^{-1} for all MgO contents. From this figure, the infrared transmission spectrum depends on MgO content. Absorption bands have been observed [6] in the infrared transmission at (i) 1300 cm^{-1} which is due to P = O stretching, (ii) 1100 cm^{-1} due to ionic P–O stretching in the middle PO_2 groups and/or the PO_3 end groups, (iii) 920 cm^{-1} due to P–O–P and/or P–O–H stretching, and (iv) 750 cm^{-1} due to P–O–P bending bond.

Regarding our results in Fig. 8, the position of the absorption bands are shifted from the above

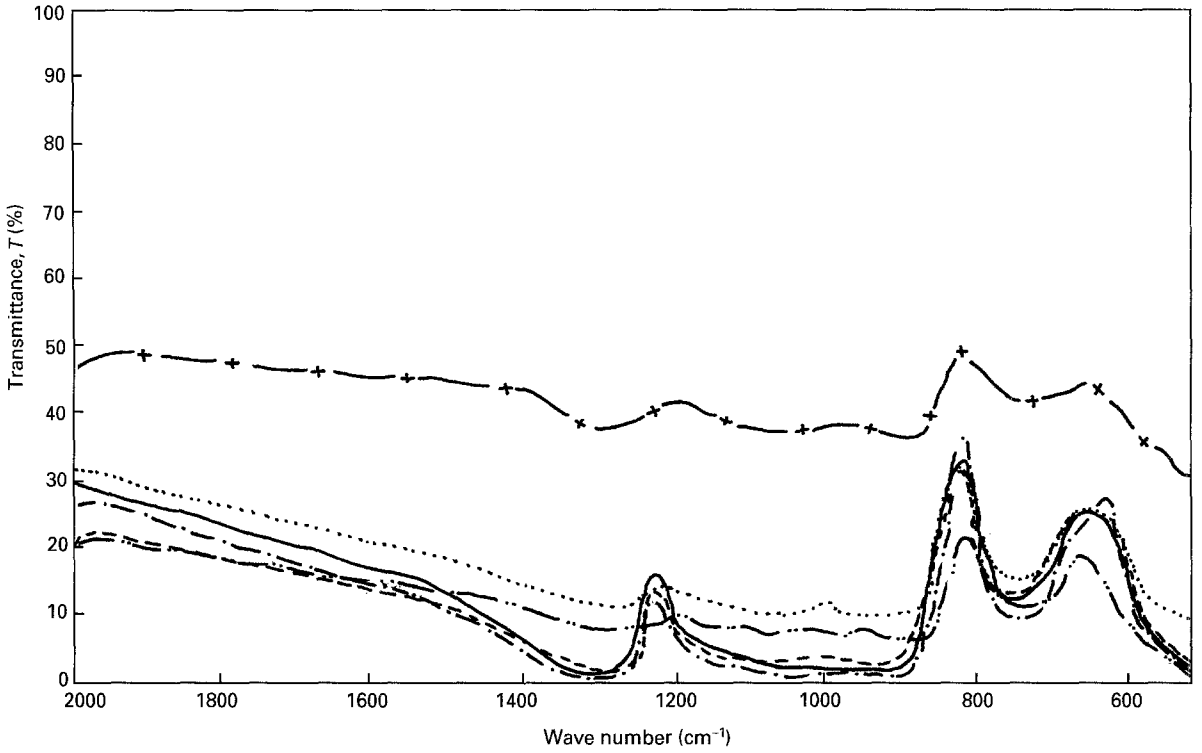

Figure 8 Infrared transmission spectrum for $MgO-P_2O_5$ glasses. (———) 20% (– – –) 25% (—·—·—) 30% (----) 35% (— + —) 40% (—··—) 45%

values, and this may be due to the chemical reaction occurring between MgO and P_2O_5 oxides.

3.4. The optical constants

The optical properties of crystalline solids have been well established using the reflectance technique. The Kramers–Kronig relation [23–26], which connects the modulus and phase of the complex Fresnel equation for normal incidence radiation, is then applied to derive the absorption data from the reflectance spectrum. The Kramers–Kronig dispersion relation was deduced under very general conditions [27], as follows

$$\varepsilon_1(\omega) = 1 + 2/\pi \int_0^\infty \frac{\zeta \varepsilon_2(\zeta)\, d\zeta}{\zeta - \omega^2} \quad (9)$$

where ε_1 is the real part of the dielectric constant.

To obtain n, and k, frequency ω and thus ε_1, ε_2 and $\alpha(\omega)$, are

$$\varepsilon_1 = n^2 - k^2 \quad (10)$$

$$\varepsilon_2 = 2nk \quad (11)$$

$$\alpha(\omega) = 4\pi k \lambda^{-1} = \varepsilon_2(\omega)\, \omega / cn(\omega) \quad (12)$$

The Kramers–Kronig relation is also valid for amorphous thin films and glasses and liquids, as well as for crystals in the ultraviolet region [28, 29]. In this work we use the modified Kramers–Kronig relation from transmission spectrum in the infrared region [30] as follows

$$n^2 = 1 + \frac{c^2\alpha^2}{16\pi^2\nu^2} + \frac{C\alpha(\nu_1)}{2\pi^2\nu} \ln\left(\frac{\nu_1 + \nu}{\nu_1 - \nu}\right) + \frac{c\alpha}{\pi^2\nu} + \frac{c}{\pi^2} \int_{\nu_0}^{\nu_1} \frac{\alpha(\nu_*)}{\nu_*^2 - \nu^2}\, d\nu_* \quad (13)$$

where ν is the frequency.

The trapezoidal rule method has been used to solve the integration of Equation 13 and n has then been computed.

Figs 9 and 10 show the variation of refractive index, n, from Equation 13 and extinction coefficient, k, as a function of wave number for the infrared region over the wave number range 500–1200 cm^{-1}. From these figures we observe that (n, k) depends on MgO content, and also, we find peaks in (n, k) values when plotted against wavelength in nearly the same position as the absorption bands found in the transmittance spectrum for the infrared region of $MgO-P_2O_5$ glasses (Fig. 8). The values of (n, k) are listed in Table II.

The Kramers–Kronig relation is used to find optical constants (n, k) for the infrared region of many glassy materials. For example, in quartz glass [31], the value of n lies between 0.438 and 2.95 and for k between 0.023 and 2.56 over the wave number range 500–1200 cm^{-1}. For comparison, we calculated (n, k) from Equation 13 for quartz glass in the infrared region with the same wave number range above, using data from [32]. The results were within − 0.01 of the above values of (n, k) for quartz glass, as shown in Table III.

3.5. a.c. conduction

Fig. 11 shows the frequency dependence of conductivity at different composition of $MgO-P_2O_5$ glass. The frequency variation of a.c. conductivity can be approximated by the equation

$$\sigma_{a.c.} = \sigma_{d.c.} + A\omega^s \quad (14)$$

where A is a constant and $s < 1$. The index s is predicted to be temperature-dependent, increasing to unity as the temperature is lowered [33].

Fig. 12 shows the variation of the dielectric loss, tan δ, with frequency at different compositions. The tangent of the loss angle is the ratio of the loss factor ε_2 as shown in Fig. 13 and the low-frequency dielectric constant, ε_1, as shown in Fig. 14 of the dielectric materials.

The increase of $\sigma_{a.c.}$ with frequency is associated with a relaxation time of various microscopic models of the conduction mechanism. One of the dominant approaches is the explanation in terms of distribution of energy barriers in which $\sigma_{a.c.}$ is caused by hopping

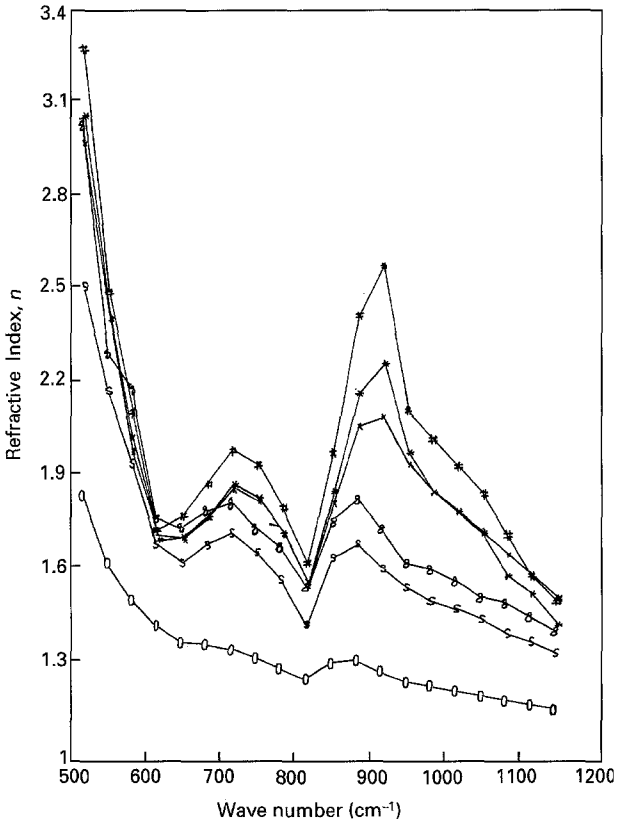

Figure 9 The relation between refractive index, *n*, and wave number in the infrared region for $MgO–P_2O_5$ glasses. MgO: (*) 20%, (+) 25%, (#) 30%, (*s*) 40%, (○) 45%, (&) 50%.

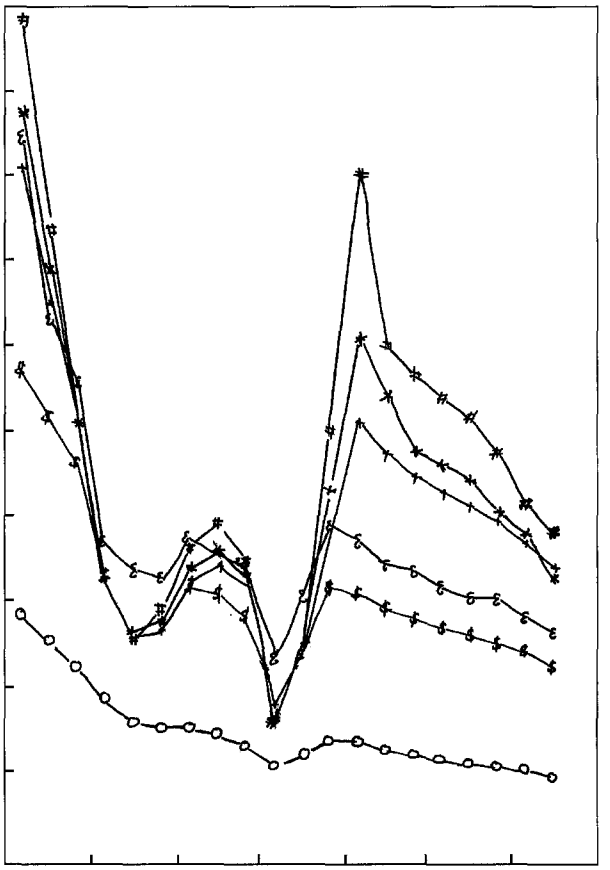

Figure 10 The relation between extinction coefficient, *k*, and wave number in the infrared region for $MgO–P_2O_5$ glasses.

TABLE II Calculated values of *n* and *k* for $MgO–P_2O_5$ glasses in the infrared region using Equation 13

Wave number (cm^{-1})	MgO											
	20%		25%		30%		40%		45%		50%	
	n	*k*	*n*	*k*	*n*	*k*	*n*	*k*	*n*	*k*	*n*	*k*
1183.3	1.35	0.606	1.36	0.548	1.38	0.662	1.31	0.437	1.15	0.199	1.38	0.529
1150	1.43	0.674	1.52	0.698	1.51	0.783	1.34	0.465	1.16	0.207	1.41	0.542
1116.6	1.53	0.776	1.58	0.757	1.58	0.848	1.38	0.502	1.18	0.222	1.46	0.580
1083.3	1.58	0.826	1.66	0.806	1.72	0.967	1.40	0.518	1.19	0.230	1.51	0.624
1050	1.72	0.901	1.73	0.840	1.85	1.04	1.45	0.537	1.20	0.235	1.52	0.624
1016.6	1.79	0.937	1.79	0.873	1.94	1.09	1.48	0.552	1.22	0.245	1.57	0.647
983.3	1.85	0.969	1.85	0.908	2.02	1.14	1.50	0.573	1.23	0.254	1.60	0.687
950	1.98	1.09	1.94	0.962	2.12	1.21	1.55	0.597	1.24	0.264	1.62	0.696
916.6	2.27	1.23	2.09	1.03	2.57	1.61	1.60	0.629	1.27	0.281	1.73	0.758
883.3	2.17	0.877	2.06	0.782	2.42	1.00	1.68	0.644	1.31	0.283	1.82	0.791
850	1.85	0.512	1.81	0.473	1.97	0.510	1.63	0.486	1.30	0.249	1.75	0.624
816.6	1.54	0.360	1.55	0.378	1.61	0.330	1.41	0.373	1.24	0.222	1.54	0.478
783.3	1.71	0.658	1.72	0.644	1.80	0.702	1.56	0.576	1.27	0.271	1.66	0.678
750	1.82	0.726	1.81	0.691	1.93	0.792	1.65	0.625	1.31	0.293	1.73	0.713
716.6	1.87	0.688	1.86	0.657	1.98	0.732	1.71	0.639	1.33	0.310	1.81	0.752
683.3	1.77	0.561	1.76	0.533	1.87	0.587	1.67	0.538	1.35	0.308	1.78	0.659
650	1.69	0.533	1.69	0.526	1.76	0.516	1.61	0.531	1.35	0.319	1.72	0.681
616.6	1.68	0.667	1.70	0.678	1.72	0.651	1.67	0.659	1.40	0.376	1.75	0.742
583.3	1.97	1.02	2.01	1.03	2.10	1.10	1.93	0.925	1.49	0.449	2.17	1.26
550	2.40	1.38	2.39	1.30	2.48	1.47	2.16	1.03	1.61	0.506	2.28	1.11
516.6	3.05	1.75	2.96	1.62	3.26	1.97	2.50	1.14	1.82	0.571	3.02	1.69

TABLE III Calculated values of n and k for glasses in the infrared region using Kramers–Kronig relation (Equation 13)

Wave number (cm^{-1})	Data from [31]		Data from [32]	
	n	k	n	k
1200	0.438	0.736	0.440	0.737
1170	0.447	0.954	0.439	0.960
1140	0.381	1.38	0.379	1.40
1110	0.671	2.35	0.683	2.37
1091	1.73	2.56	1.70	2.53
1070	2.59	2.06	2.61	2.04
1050	2.95	1.37	2.98	1.39
1015	2.74	0.237	2.72	0.240
1000	2.42	0.145	2.40	0.142
960	2.03	0.088	2.05	0.091
940	1.90	0.050	1.92	0.048
920	1.81	0.023	1.80	0.024
901	1.77	0.023	1.76	0.022
885	1.71	0.025	1.70	0.027
870	1.69	0.026	1.71	0.030
862	1.68	0.060	1.69	0.062
840	1.64	0.200	1.63	0.220
820	1.64	0.284	1.66	0.285
800	1.77	0.344	1.79	0.343
775	1.84	0.170	1.83	0.169
752	1.72	0.080	1.71	0.078
741	1.70	0.065	1.71	0.066
714	1.66	0.045	1.65	0.047
690	1.60	0.033	1.61	0.034
667	1.54	0.032	1.55	0.031
645	1.52	0.032	1.51	0.034
625	1.46	0.035	1.48	0.036
606	1.44	0.047	1.42	0.049
588	1.41	0.050	1.42	0.048
571	1.35	0.060	1.37	0.063
552	1.23	0.085	1.20	0.086
529	1.05	0.200	1.06	0.220
500	0.647	0.751	0.670	0.750

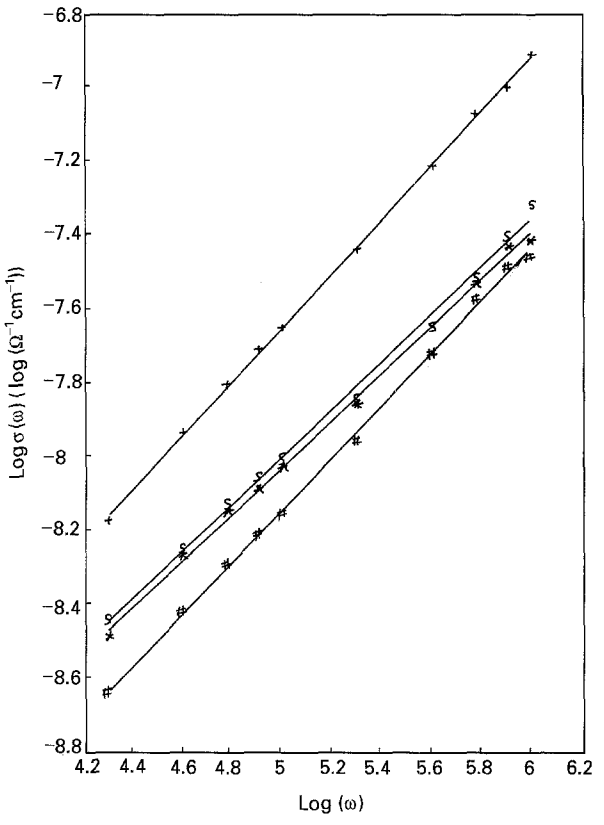

Figure 11 The relation between a.c. conductivity and frequency for $X = 20$–40 of MgO–P_2O_5 glasses. MgO: (*) 20%, $s = 0.64$; (s) 25%, $s = 0.65$; (#) 30%, $s = 0.71$; (+) 40%, $s = 0.73$.

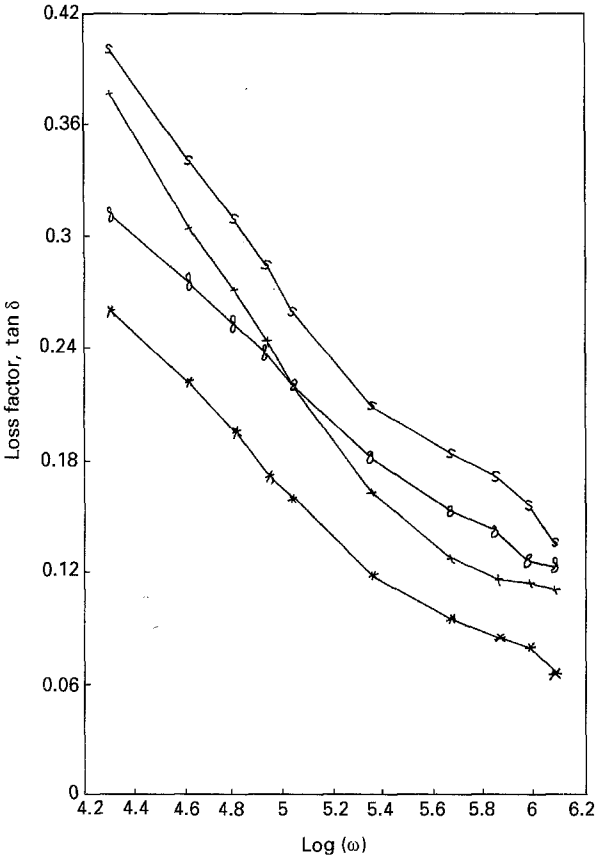

Figure 12 The relation between loss factor, tan δ and frequency for $X = 20$–40 of MgO–P_2O_5 glasses. MgO: (*) 20%, (+) 25%, (s) 30%, (&) 40%.

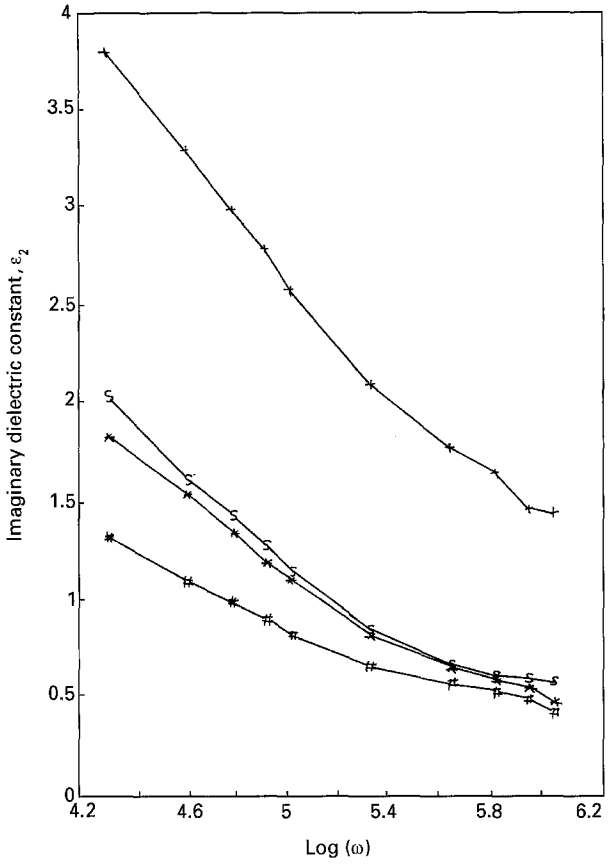

Figure 13 The relation between imaginary dielectric constant, ε_2, and frequency for $X = 20$–40 of MgO–P_2O_5 glasses. MgO: (*) 20%, (*s*) 25%, (#) 30%, (+) 40%.

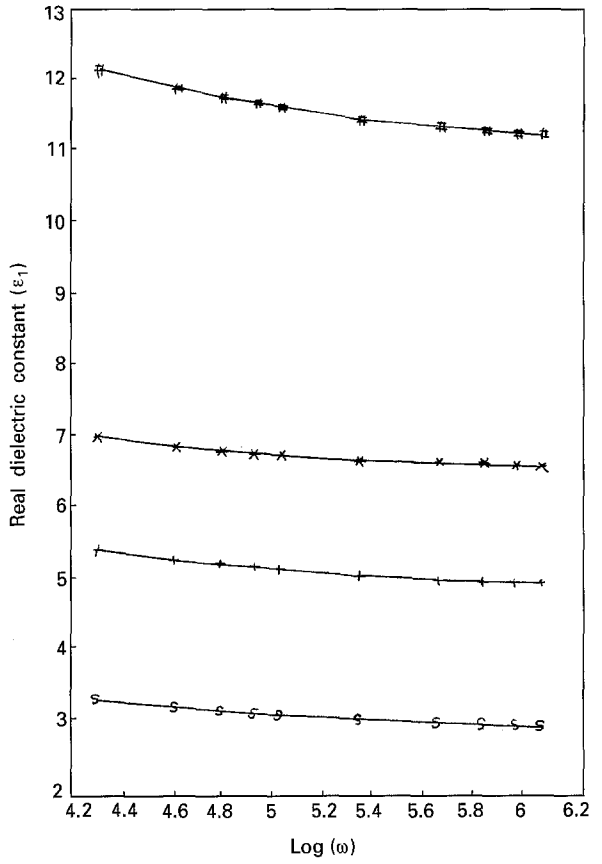

Figure 14 The relation between real dielectric constant, ε_1, and frequency for $X = 20$–40 of MgO–P_2O_5 glasses. MgO: (*) 20%, (+) 25%, (*s*) 30%, (#) 40%.

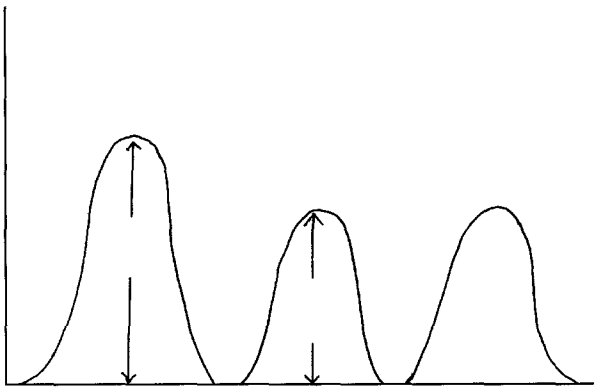

Figure 15 Simplified model of energy barrier distribution for a.c. and d.c. conduction, showing different barrier heights.

of charge carriers over a small barrier of height, H_2, while $\sigma_{d.c.}$ is caused by hops over a large barrier height, H_1, as indicated in Fig. 15 [34].

In conclusion, because of the growing technological importance of phosphate glasses [35], particularly magnesium and calcium phosphate glasses [36, 37], an understanding of various properties is needed. The main purpose of this paper was to present some of those properties.

References

1. N. F. MOTT and E. A. DAVIS, "Electronic Processes in Non-Crystalline Materials", (Clarendon Press, Oxford, 1979).
2. S. P. EDIRISINGHE and C. A. HOGARTH, *J. Mater. Sci. Lett.* **8** (1989) 789.
3. S. K. J. AL-ANI, PhD thesis, Brunel University (1984).
4. S. K. J. AL-ANI and A. A. HIGAZY, *J. Mater. Sci.* **26** (1991), 3670.
5. E. KORDES, W. VOGEL and R. FETEROWSKY, *Z. Elektrochem*, **57** (1953) 282.
6. T. OKURA, K. YAMASHITA and T. KANAZAWA, *Phys. Chem. Glasses* **29** (1988) 13.
7. F. URBACH, *Phys. Rev.* **92** (1953) 1324.
8. J. TAUC, R. GIGOROVICI and A. VANCU, *Phys. Status Solidi* **15** (1966) 627.
9. E. A. DAVIS and N. F. MOTT, *Philos. Mag.* **22** (1970) 903.
10. E. A. DAVIS, *J. Non-Cryst. Solids* **4** (1970) 107.
11. S. K. J. AL-ANI and C. A. HOGARTH, *ibid.* **69** (1984) 167.
12. *Idem, Phys. Status Solidi (a)* **87** (1985) K65.
13. C. A. HOGARTH and M. Y. NADEEM, *ibid.* **68** (1981) K181.
14. S. K. J. AL-ANI, KI. ARSHAK and C. A. HOGARTH, *J. Mater. Sci.* **19** (1984) 1737.
15. S. K. J. AL-ANI, C. A. HOGARTH and M. ILYAS, *J. Mater. Sci. Lett.* **3** (1984) 391.
16. G. R. MORIDI and C. A. HOGARTH, in "Proceedings of the 7th International Conference on Amorphous and Liquid Semiconductors", Edinburgh, edited by W. E. Spear (1977) 688.
17. S. K. J. AL-ANI, C. A. HOGARTH and R. A. EL-MALAWANY, *J. Mater. Sci.* **20** (1985) 661.
18. S. K. J. AL-ANI and C. A. HOGARTH, *ibid.* **20** (1985) 1185.
19. G. W. ANDERSON and W. D. COMPTON, *J. Chem. Phys.* **52** (1970) 6166.
20. V. VORLIČEK, M. LAVETOVA, S. K. PAVLOV and L. PAJASOVA, *J. Non-Cryst. Solids* **45** (1981) 289.
21. I. D. DOW and D. REDFIELD, *Phys. Rev. B* **5** (1972) 594.
22. J. TAUC, in "Optical Properties of Solids", edited by F. Abeles (Amsterdam, 1970) p. 277.
23. H. A. KRAMERS, *Atticong. Int. Fis. Comr.* **2** (1927) 545.
24. *Idem, Phys. Z.* **30** (1929) 521.

25. R. De L. KRONIG, *J. Opt. Soc. Am.* **12** (1926) 547.
26. *Idem, Phys. Rev.* **30** (1929) 521.
27. J. TAUC, *Prog. Semicond.* **9** (1965) 87.
28. J. TAUC, (ed.), "Amorphous and Liquid Semiconductors" (Plenum Press, London, 1974).
29. J. WONG and C. A. ANGELL, "Glass structure by spectroscopy" (Marcel Dekker, New York, 1977).
30. I. J. DAYAWANZA, PhD thesis, University of Wales (1977).
31. T. R. STERYER, L. DAY and D. R. HUFMAN, *Appl. Opt.* **13** (1974) 1586.
32. Q. S. MAJEED, PhD thesis, University of Wales, (1990).
33. S. R. ELLIOT, *Philos. Mag.* **36** (1977) 1291.
34. A. DOI, *J. Mater. Sci. Lett.* **6** (1987) 648.
35. W. MATZ, D. STACHEL and E. A. GOREMYCHKIN, *J. Non-Cryst. Solids* **101** (1988) 80.
36. M. ASHIZUKA, E. ISHIDA, S. UTO and R. C. BRADT, *ibid.* **104** (1988) 316.
37. E. MATSUBARA, T. KAWAZOE, Y. WASEDA, M. ASHIZUKA and E. ISIDA, *J. Mater. Sci.* **23** (1988) 547.

Received 13 January 1993
and accepted 22 July 1994